Electronic Supplementary Material (ESI) for Dalton Transactions.
This journal is © The Royal Society of Chemistry 2020

Electronic Supplementary Information

for

Molecular Enneanuclear Cu^{II} Phosphates Containing Planar Hexanuclear and Trinuclear Sub-Units: Syntheses, Structures, and Magnetism

Biswajit Santra,[a] Pankaj Kalita,[b] Shubhadeep Chandra,[c] Debdeep Mandal,[a] Vierandra Kumar,[d] R. Surya Narayanan,[a] Atanu Dey,[a] Nicolas Chrysochos,[e] Volker Huch,[f] Sourav Biswas,[g] Debajyoti Ghoshal,[g] E. Carolina Sañudo,*[h,i] Biprajit Sarkar,*[c] Carola Schulzke,*[e] Vadapalli Chandrasekhar,*[a,d] and Anukul Jana*[a]*

[a]Tata Institute of Fundamental Research Hyderabad, Gopanpally, Hyderabad-500107, India
[b]National Institute of Science Education and Research Bhubaneswar, HBNI, Bhubaneswar-752050, Odisha, India
[c]Institut für Chemie und Biochemie, Anorganische Chemie, Freie Universität Berlin, Fabeckstraße 34–36,14195, Berlin, Germany, E-mail: biprajit.sarkar@fu-berlin.de
[d]Department of Chemistry, Indian Institute of Technology Kanpur, Kanpur 208016, India
[e]Institut für Biochemie, Universität Greifswald, Felix-Hausdorff-Straße 4, D-17487 Greifswald, Germany
[f]Krupp-Chair of General and Inorganic Chemistry, Saarland University, 66123 Saarbrücken, Germany
[g]Department of Chemistry, Jadavpur University, Jadavpur, Kolkata-32, India, E-mail: dghoshal@chemistry.jdvu.ac.in
[h]Departament de Química Inorgànica i Orgànica, Secció de Química Inorgànica, Facultat de Química, Universitat de Barcelona, Diagonal 645, 08028 Barcelona, Spain
[i]Institut de Nanociència i Nanotecnologia, Universitat de Barcelona, Diagonal 645, 08028 Barcelona, Spain

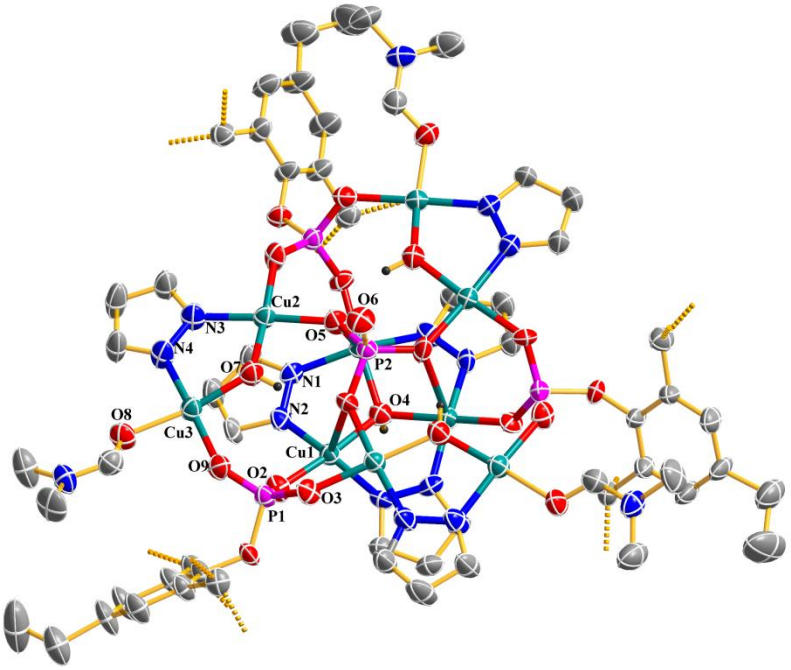

Figure S1. Molecular structure of $\mathbf{2}^{\mathbf{EtAr}}$

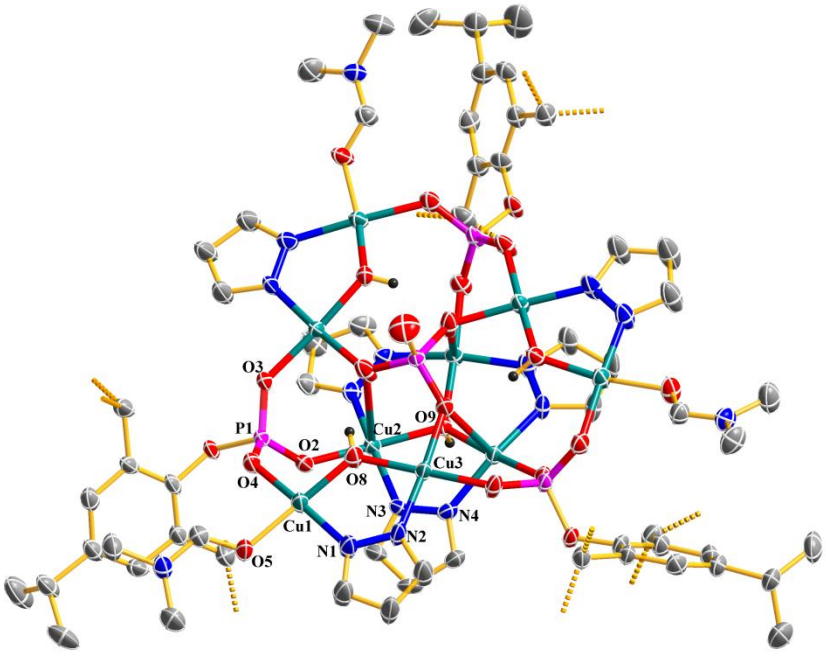

Figure S2. Molecular structure of $\mathbf{2}^{\mathbf{\textit{i}PrAr}}$

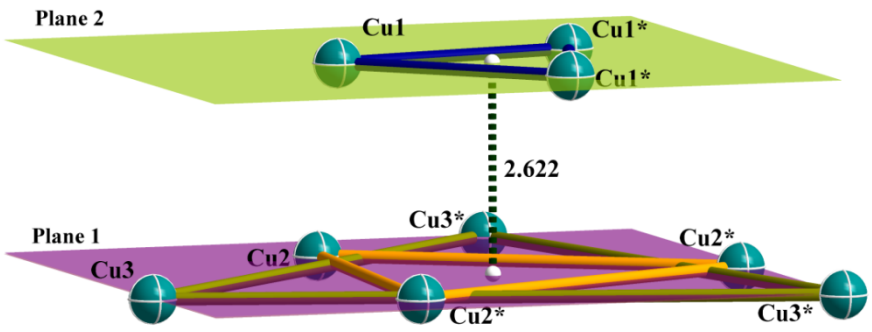

Figure S3. Mean plane analysis for compound $\mathbf{2}^{\mathbf{EtAr}}$.

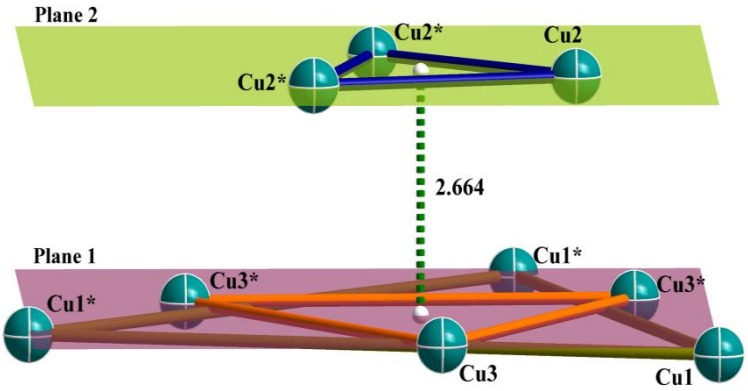

Figure S4. Mean plane analysis for compound $\mathbf{2}^{\mathbf{\textit{i}PrAr}}$.

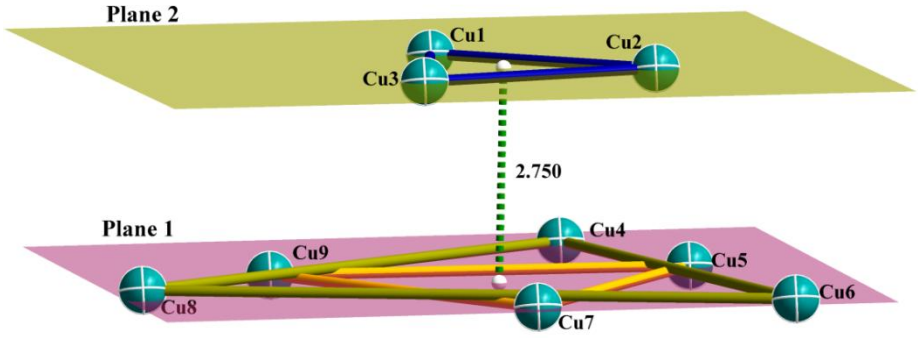

Figure S5. Mean plane analysis for compound $\mathbf{2}^{\mathbf{Dip}}$

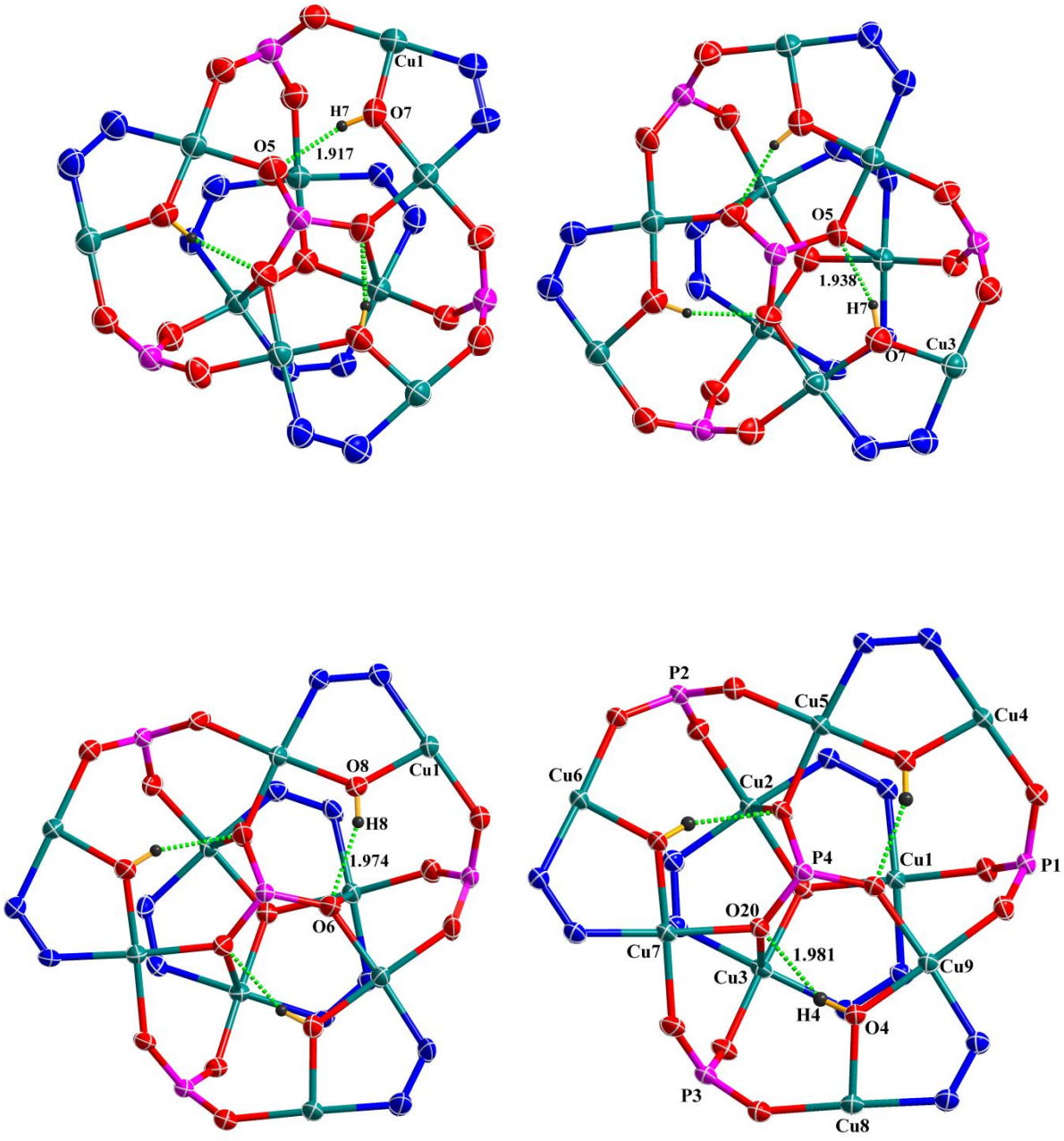

Figure S6. H-bonded core view of $\mathbf{2}^{\mathbf{MeAr}}$ (top left), $\mathbf{2}^{\mathbf{EtAr}}$ (top right), $\mathbf{2}^{\mathbf{iPrAr}}$ (bottom left), and $\mathbf{2}^{\mathbf{Dip}}$ (bottom right).

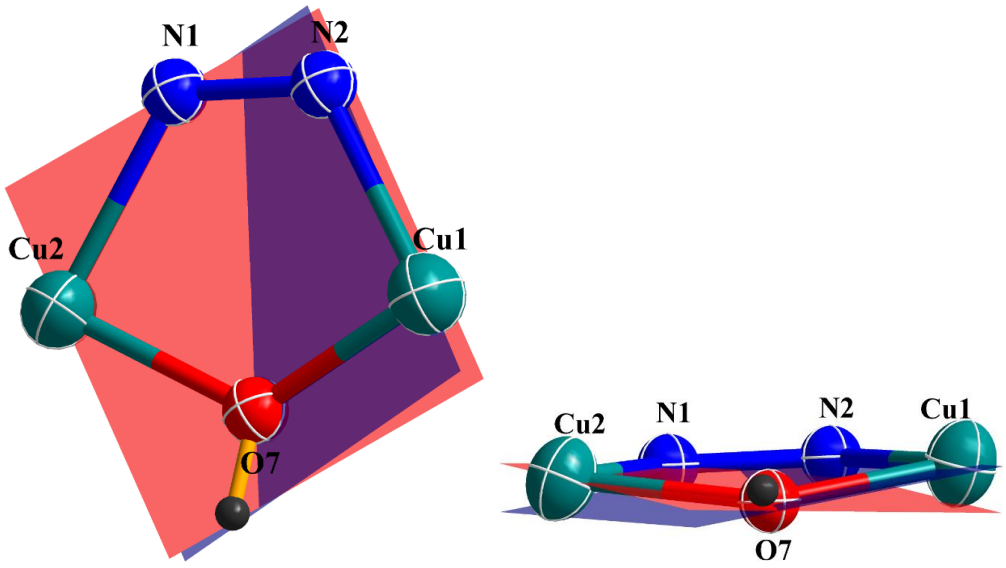

Figure S7. A non-planar view (dihedral angle between the two planes is 11.158°) of five membered ring comprising two copper centres, one oxygen (OH) and two nitrogen atoms (pyrazolate) of $\mathbf{2}^{\mathbf{MeAr}}$.

Table S1. Cu…Cu separations of $\mathbf{2}^{\mathbf{MeAr}}$, $\mathbf{2}^{\mathbf{EtAr}}$, $\mathbf{2}^{\mathbf{iPrAr}}$, and $\mathbf{2}^{\mathbf{Dip}}$.

Compound	Cu…Cu separation in same triangular plane	Distance between plane 1 and plane 2	Proximal Cu…Cu Separation between plane 1 and plane 2
$\mathbf{2}^{\mathbf{MeAr}}$	3.344(5) (plane 1) 5.261(8) (plane 1) 5.451(6) (plane 1) 3.309(4) (plane 2)	2.635	3.506(4)
$\mathbf{2}^{\mathbf{EtAr}}$	3.349(3) (plane 1) 5.273(6) (plane 1) 5.463(6) (plane 1) 3.318(5) (plane 2)	2.622	3.497(4)
$\mathbf{2}^{\mathbf{iPrAr}}$	3.354(1) (plane 1) 5.271(1) (plane 1) 5.443(1) (plane 1) 3.323(1) (plane 2)	2.644	3.528(1)
$\mathbf{2}^{\mathbf{Dip}}$	3.339(9) (plane 1) 5.239(2) (plane 1) 5.461(1) (plane 1) 5.398(1) (plane 1) 5.437(2) (plane 1) 5.256(1) (plane 1) 5.232(1) (plane 1) 3.355(8) (plane 2) 3.372(8) (plane 2) 3.372(9) (plane 2)	2.750	3.353(7)

Table S2. H-Bonding Parameters of $\mathbf{2}^{\mathbf{MeAr}}$, $\mathbf{2}^{\mathbf{EtAr}}$, $\mathbf{2}^{\mathbf{iPrAr}}$, and $\mathbf{2}^{\mathbf{Dip}}$.

Compound	D–H....A	D–H (Å)	H...A (Å)	D...A (Å)	D–H...A (º)
$\mathbf{2}^{\mathbf{MeAr}}$	**O**(7)–**H**(7)....**O**(5)	0.83(4)	1.92(5)	2.731(7)	166(5)
$\mathbf{2}^{\mathbf{EtAr}}$	**O**(7)–**H**(7)....**O**(5)	0.83(13)	1.94(13)	2.735(11)	161(11)
$\mathbf{2}^{\mathbf{iPrAr}}$	**O**(8)–**H**(8)....**O**(6)	0.80(5)	1.98(5)	2.736(7)	157(6)
$\mathbf{2}^{\mathbf{Dip}}$	**O**(2)–**H**(2)....**O**(21)	0.82(3)0.81(4)	1.94(3)	2.725(4)	159(3)
	O(3)–**H**(3)....**O**(22)	0.82(3)	2.00(4)	2.756(4)	156(4)
	O(4)–**H**(4)....**O**(20)	0.80(4)	1.98(2)	2.746(4)	155(4)
	O(1)–**H**(1)....**O**(24)		1.97(4)	2.668(4)	145(4)

Table S3. Selected bond lengths (Å) and bond angle (°) parameters for $\mathbf{2}^{\mathbf{MeAr}}$

Coordination Geometry	**Bond lengths** (Å)	**Bond angles** (°)
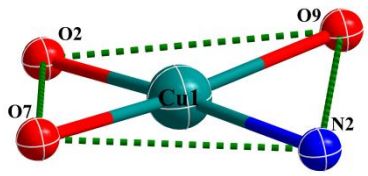	Cu1–O7 1.867(4) Cu1–O2 1.928(4) Cu1–N2 1.937(5) Cu1–O9 1.976(4)	O7–Cu1–O2 95.72(17) O7–Cu1–N2 85.7(2) O7–Cu1–O9 170.8(2) O2–Cu1–N2 175.5(2) O2–Cu1–O9 89.86(18) N2–Cu1–O9 89.3(2)
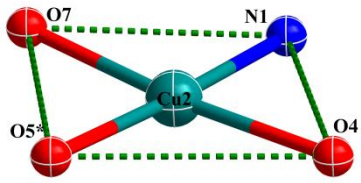	Cu2–O7 1.883(4) Cu2–N1 1.934(5) Cu2–O5* 1.957(4) Cu2–O4 1.959(4)	O7–Cu2–N1 85.2(2) O7–Cu2–O5* 91.38(18) N1–Cu2–O5* 176.6(2) O7–Cu2–O4 75.26(19) N1–Cu2–O4 92.61(19) O5*–Cu2–O4 90.77(17)
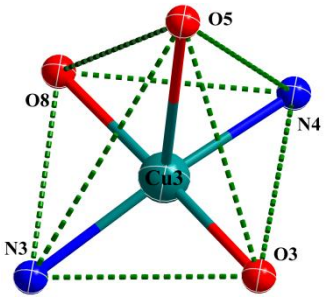	Cu3–O5 2.840(5) Cu3–O3 1.896(4) Cu3–N4 1.936(5) Cu3–N3 1.938(5) Cu3–O8 1.9558(18)	O3–Cu3–N4 94.77(19) O3–Cu3–N3 91.02(18) O3–Cu3–O8 174.6(2) N4–Cu3–O8 88.42(14) N4–Cu3–N3 163.9(2) N3–Cu3–O8 87.06(15)

*1+Y-X,1-X,+Z

Table S4. Selected bond lengths (Å) and bond angle (°) parameters for **2**$^{\mathbf{EtAr}}$

Coordination Geometry	**Bond lengths** (Å)	**Bond angles** (°)
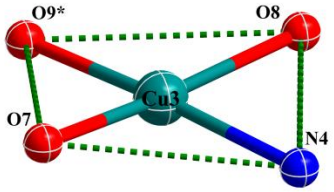	Cu3–O7 1.871(7) Cu3–N4 1.941(8) Cu3–O9* 1.943(7) Cu3–O8 1.985(7)	O7–Cu3–N4 86.3(3) O7–Cu3–O9* 95.6(3) N4–Cu3–O9* 175.3(4) O7–Cu3–O8 170.3(3) N4–Cu3–O8 88.5(3) O9*–Cu3–O8 90.2(3)
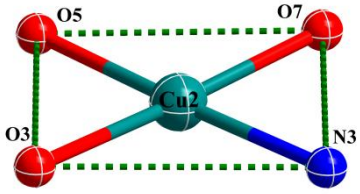	Cu2–O7 1.886(7) Cu2–N3 1.933(8) Cu2–O3 1.944(6) Cu2–O5 1.956(7)	O7–Cu2–N3 85.4(3) O7–Cu2–O3 175.7(3) N3–Cu2–O3 92.7(3) O7–Cu2–O5 91.3(3) N3–Cu2–O5 176.7(3) O3–Cu2–O5 90.6(3)
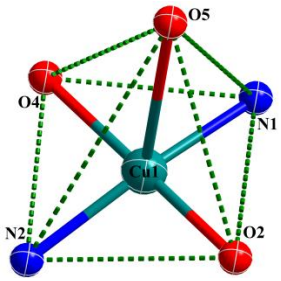	Cu1–O5 2.799(8) Cu1–O2 1.905(6) Cu1–N2 1.927(8) Cu1–N1 1.932(8) Cu1–O4 1.956(2)	O2–Cu1–N2 91.4(3) O2–Cu1–N1 94.6(3) N2–Cu1–N1 163.6(3) O2–Cu1–O4 174.6(3) N2–Cu1–O4 87.0(2) N1–Cu1–O4 88.3(2)

*1+Y-X,1-X,+Z

Table S5. Selected bond lengths (Å) and bond angle (°) parameters for **2**$^{\mathbf{\textit{i}PrAr}}$

Coordination Geometry	**Bond lengths** (Å)	**Bond angles** (°)
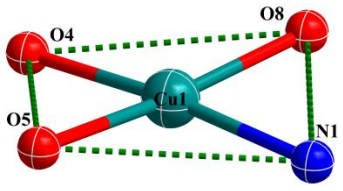	Cu1–O8 1.870(4) Cu1–O4 1.943(4) Cu1–N1 1.948(5) Cu1–O5 1.983(4)	O8–Cu1–O4 95.96(16) O8–Cu1–N1 85.27(18) O4–Cu1–N1 174.4(2) O8–Cu1–O5 169.79(19) O4–Cu1–O5 89.81(15) N1–Cu1–O5 89.79(17)
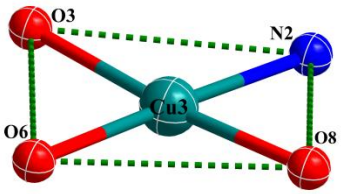	Cu3–O8 1.892(4) Cu3–N2 1.932(5) Cu3–O6* 1.943(4) Cu3–O3 1.948(3)	O8–Cu3–N2 84.90(17) O8–Cu3–O6* 91.77(16) N2–Cu3–O6* 176.63(17) O8–Cu3–O3 175.26(19) N2–Cu3–O3 3.11(17) O6*–Cu3–O3 90.17(15)

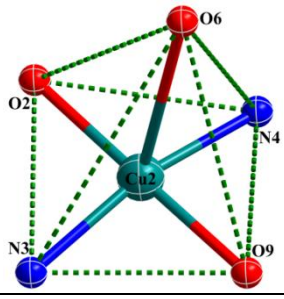	Cu2–O6 2.829(5) Cu2–O2 1.910(4) Cu2–N3 1.945(4) Cu2–N4 1.950(4) Cu2–O9 1.9630(16)	O2–Cu2–N3 91.21(16) O2–Cu2–N4 94.61(17) N3–Cu2–N4 165.6(2) O2–Cu2–O9 175.0(2) N3–Cu2–O9 87.37(13) N4–Cu2–O9 87.88(14)

*1+Y-X,1-X,+Z

Table S6. Selected bond lengths (Å) and bond angle (°) parameters for $\mathbf{2^{Dip}}$

Coordination Geometry	**Bond lengths** (Å)	**Bond angles** (°)
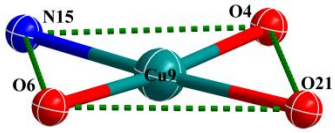	Cu9–O4 1.887(3) Cu9–O6 1.941(3) Cu9–N15 1.947(3) Cu9–O21 1.947(3)	O4–Cu9–O6 174.43(13) O4–Cu9–N15 85.77(12) O6–Cu9–N15 94.78(12) O4–Cu9–O21 90.54(11) O6–Cu9–O21 88.79(11) N15–Cu9–O21 176.18(12)
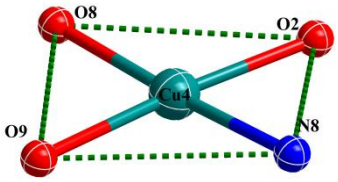	Cu4–O2 1.846(3) Cu4–O9 1.945(3) Cu4–O8 1.948(3) Cu4–N8 1.985(3)	O2–Cu4–O9 173.15(13) O2–Cu4–O8 96.25(12) O9–Cu4–O8 90.54(12) O2–Cu4–N8 84.47(13) O9–Cu4–N8 88.70(13) O8–Cu4–N8 175.79(13)
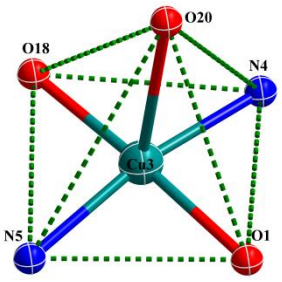	Cu3–O20 2.510(2) Cu3–O18 1.932(3) Cu3–N5 1.957(3) Cu3–N4 1.966(3) Cu3–O1 1.981(3)	O18–Cu3–N5 91.03(13) O18–Cu3–N4 93.33(12) N5–Cu3–N4 168.49(14) O18–Cu3–O1 177.25(12) N5–Cu3–O1 86.81(12) N4–Cu3–O1 88.48(12)

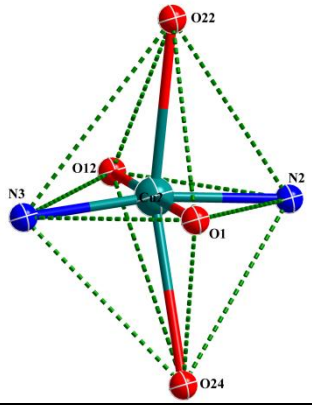	Cu2–O22 3.3329(12) Cu2–O24 3.3268(11) Cu2–N3 1.933(3) Cu2–N2 1.945(3) Cu2–O12 1.957(3) Cu2–O1 2.014(3)	N3–Cu2–N2 170.11(14) N3–Cu2–O12 91.51(12) N2–Cu2–O12 92.99(12) N3–Cu2–O1 87.78(12) N2–Cu2–O1 87.86(12) O12–Cu2–O1 178.80(12)

Table S7. Crystal and refinement data for compounds $\mathbf{2}^{\mathbf{MeAr}}$, $\mathbf{2}^{\mathbf{EtAr}}$, $\mathbf{2}^{\mathbf{\textit{i}PrAr}}$, and $\mathbf{2}^{\mathbf{Dip}}$.

Compound	$\mathbf{2}^{\mathbf{MeAr}}$	$\mathbf{2}^{\mathbf{EtAr}}$	$\mathbf{2}^{\mathbf{\textit{i}PrAr}}$	$\mathbf{2}^{\mathbf{Dip}}$
CCDC number	1835295	1835294	1835296	1835293
Empirical formula	$C_{159}H_{151}Cu_9N_{15}O_{23}P_4$	$C_{163}H_{159}Cu_9N_{15}O_{23}P_4$	$C_{167}H_{167}Cu_9N_{15}O_{23}P_4$	$C_{87}H_{139}Cu_9N_{19}O_{27}P_4$
F_w	3335.34	3391.78	3447.89	2578.90
Temp. (K)	170(2)	170(2)	150.01(10)	152(2)
Crystal system	Trigonal	Trigonal	Trigonal	Triclinic
space group	*R*3*c*	*R*3*c*	*R*3*c*	*P*-1
a (Å)	31.198(4)	31.380(4)	31.529(7)	11.159(3)
b (Å)	31.198(4)	31.380(4)	31.529(7)	22.849(6)
c (Å)	27.045(5)	27.242(5)	28.088(10)	23.684(7)
α (°)				111.62(11)
β (°)				97.08(12)
γ (°)				91.35(13)
V (Å^3)	22796(8)	23232(8)	24181.2(14)	5555(3)
Z	6	6	6	2
D_{calcd}(Mg m^{-3})	1.458	1.455	1.421	1.542
μ (mm^{-1})	1.348	1.324	1.274	1.822
θ range (°)	1.684 to 26.464	2.483 to 27.495	3.262 to 29.120	1.572 to 25.999
Reflections collected	61838	68936	21569	76022
Independent reflections	9916	11745	10717	21551
Data/ restraints/ parameters	9916 / 2 / 541	11745 / 3 / 546	10717 / 3 / 556	21551 / 15 / 1261
GOF	0.889	0.825	0.991	1.036
$R_1[I_0>2\sigma(I_0)]$	0.0376	0.0500	0.0440	0.0440
wR_2(all data)	0.0864	0.1214	0.1002	0.1216
Largest diff. peak and hole (e Å^{-3})	0.542 and −0.382	0.696 and −0.829	1.066 and −0.386	1.815 and -1.535

Chart S1. Denticity and Harris notation of ligand binding modes.

Denticity and Harris Notation of Ligand	**Compound**
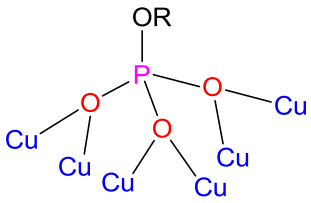 6.222 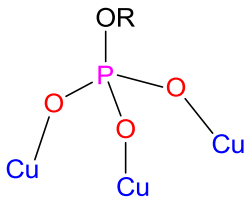 3.111	**2**^{MeAr}, **2**^{EtAr}, **2**^{iPrAr}
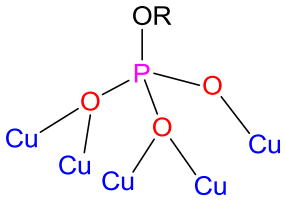 5.221 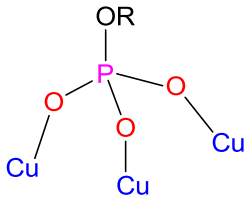 3.111	**2**^{Dip}

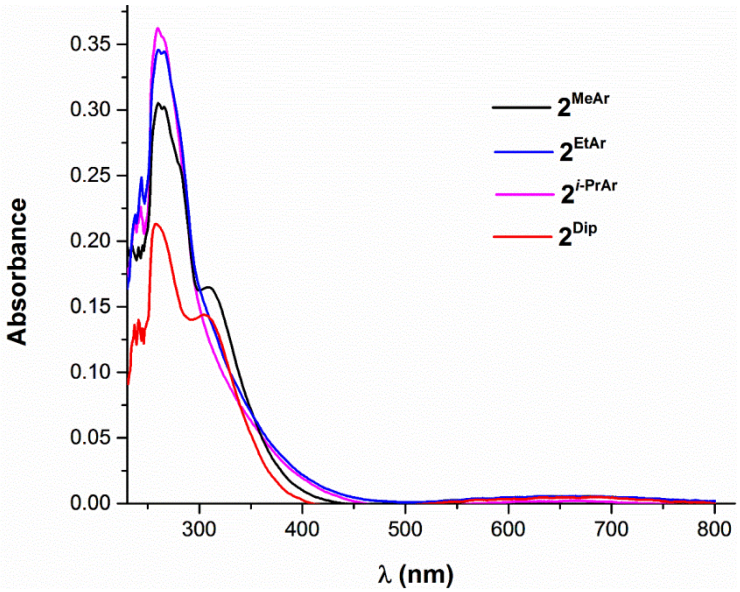

Figure S8. UV/vis spectra of $\mathbf{2}^{\mathbf{MeAr}}$, $\mathbf{2}^{\mathbf{EtAr}}$, $\mathbf{2}^{\mathbf{iPrAr}}$, and $\mathbf{2}^{\mathbf{Dip}}$.

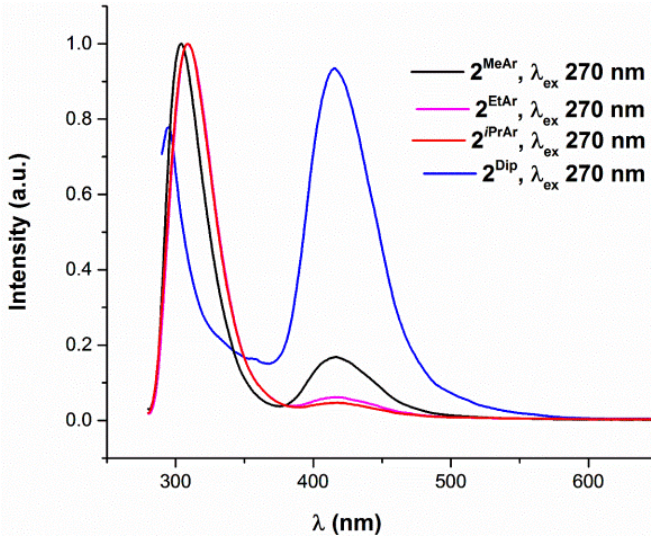

Figure S9. Emission spectra of $\mathbf{2}^{\mathbf{MeAr}}$, $\mathbf{2}^{\mathbf{EtAr}}$, $\mathbf{2}^{\mathbf{iPrAr}}$, and $\mathbf{2}^{\mathbf{Dip}}$ (λ_{ex} 270 nm).

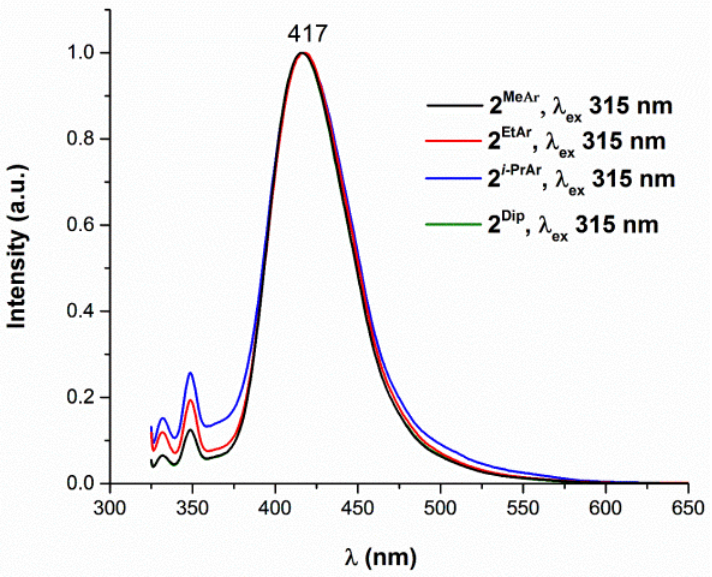

Figure S10. Emission spectra of $\mathbf{2}^{\mathbf{MeAr}}$, $\mathbf{2}^{\mathbf{EtAr}}$, $\mathbf{2}^{\mathbf{\textit{i}PrAr}}$, and $\mathbf{2}^{\mathbf{Dip}}$ (λ_{ex} 315 nm) in DMF (10^{-4} M).

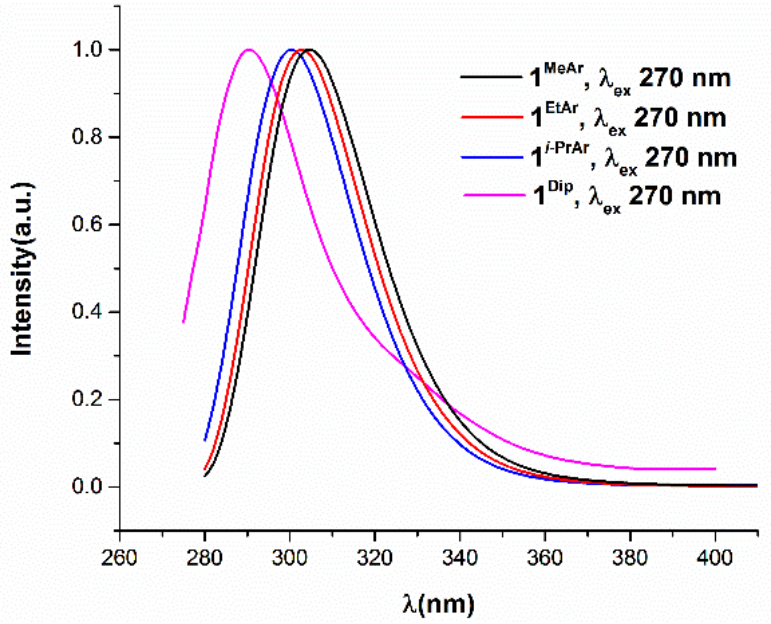

Figure S11. Emission spectra of $\mathbf{1}^{\mathbf{MeAr}}$, $\mathbf{1}^{\mathbf{EtAr}}$, $\mathbf{1}^{\mathbf{\textit{i}PrAr}}$, and $\mathbf{1}^{\mathbf{Dip}}$ (λ_{ex} 270 nm) in DMF (10^{-4} M).

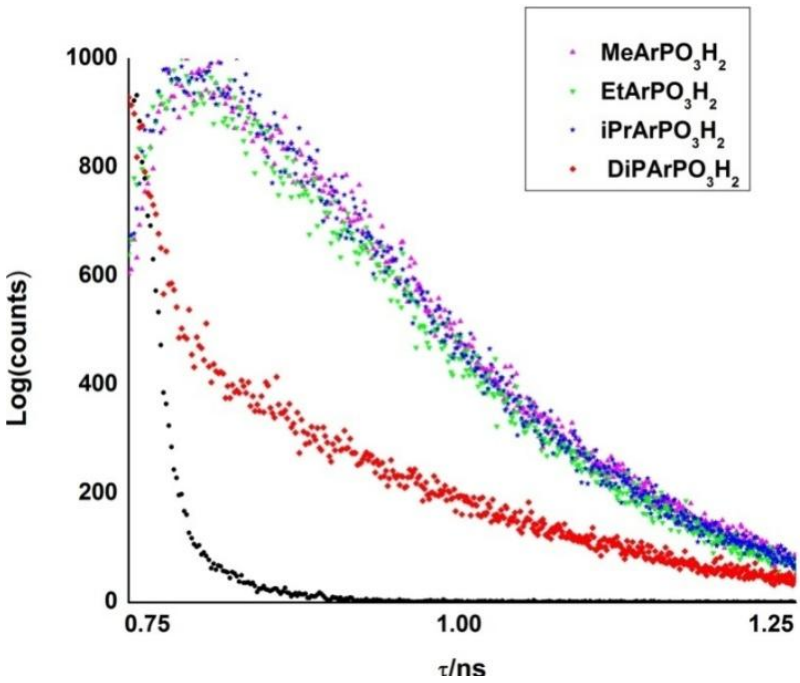

Figure S12. Luminescence decays of the ligands in DMF at 298 K ($MeArPO_3H_2$ = $\mathbf{1}^{MeAr}$, $EtArPO_3H_2$ = $\mathbf{1}^{EtAr}$, $iPrArPO_3H_2$ = $\mathbf{1}^{iPrAr}$ and $DipArPO_3H_2$ = $\mathbf{1}^{Dip}$)

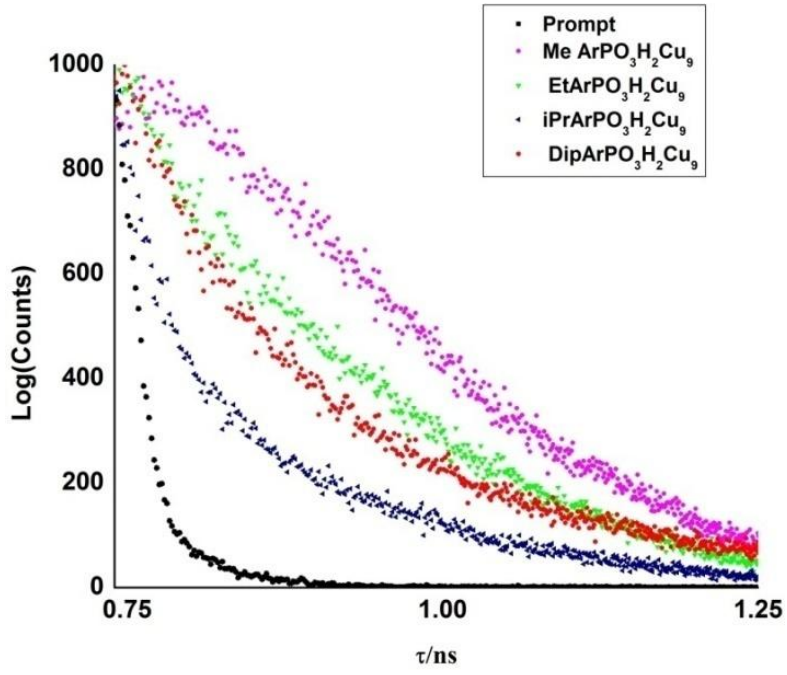

Figure S13. Luminescence decays of the Cu9-complexes in DMF at 298 K ($MeArPO_3H_2Cu_9$ = **2**^{MeAr}, $EtArPO_3H_2Cu_9$ = **2**^{EtAr}, $iPrArPO_3H_2Cu_9$ = **2**^{iPrAr} and $DipArPO_3H_2Cu_9$ = **2**^{Dip})

Table S8. UV/vis and Luminescence and life time data for ligands and their compounds in DMF

Compounds	**Solvent**	**λ_{abs} (nm)**	**$\lambda_{emission}$ (nm)**	**Lifetime (ns)**
1^{MeAr}	DMF	272, 278, 285	303	4.7
1^{EtAr}	DMF	272, 277, 284	305	4.6
1^{iPrAr}	DMF	260, 270, 279	300	4.5
1^{Dip}	DMF	260, 292	290	5.2
2^{MeAr}	DMF	260, 300, 660	304	4.7
2^{EtAr}	DMF	260, 309, 660	308	4.2
2^{iPrAr}	DMF	260, 660	308	3.9
2^{Dip}	DMF	258, 306, 660	415	8.5

Thermogravimetric Analysis

In order to understand the thermal stability of the complexes a thermogravimetric analysis (TGA) study was carried out. This reveals that weight loss occurred through two successive steps in the case of $\mathbf{2}^{\mathbf{MeAr}}$, $\mathbf{2}^{\mathbf{EtAr}}$, and $\mathbf{2}^{\mathbf{\textit{i}PrAr}}$. 9.3 % (calcd. 8.6 %), 9.5 % (calcd. 8.5 %), and 9.6 % (calcd. 8.3%) weight loss occurred for $\mathbf{2}^{\mathbf{MeAr}}$, $\mathbf{2}^{\mathbf{EtAr}}$, and $\mathbf{2}^{\mathbf{\textit{i}PrAr}}$ in the range 169–233 °C, 177−235 °C, and 175–220 °C, respectively which corresponds to the loss of coordinated DMF and hydroxide group. A major weight loss of 43.5 % (calcd. 43.2 %), 41.3 % (calcd. 43 %), and 30.4 % (calcd. 29.8 %) occurred in the range 233–401 °C, 235–466 °C, and 220–397 °C, respectively for $\mathbf{2}^{\mathbf{MeAr}}$, $\mathbf{2}^{\mathbf{EtAr}}$, and $\mathbf{2}^{\mathbf{\textit{i}PrAr}}$ due to the decomposition of pyrazole and phosphate ligand. But in case of $\mathbf{2}^{\mathbf{Dip}}$ a distinct plateau could be found at the range 194–316 °C for the major weight loss 47 % (calcd. 48 %) which corresponds to the loss of all the coordinated and non-coordinated DMF molecules as well as the decomposition of pyrazole and one phosphate ligand.

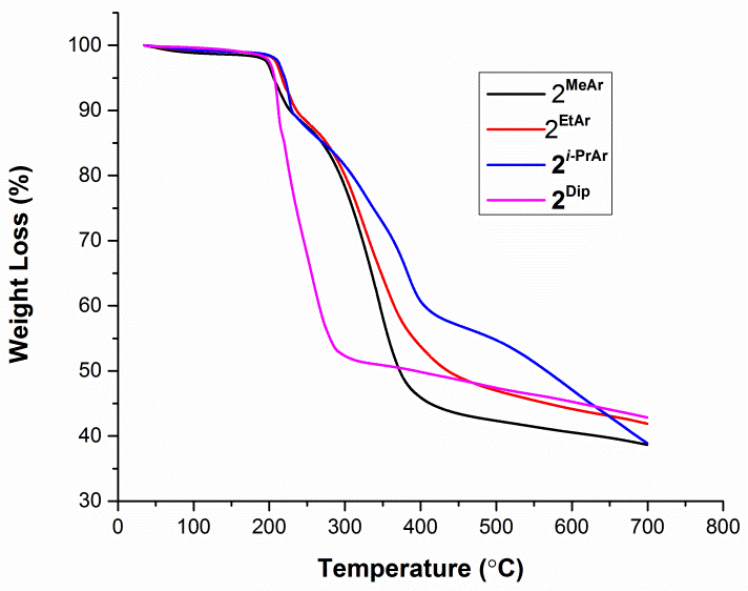

Figure S14. Thermogravimetric analysis for $\mathbf{2}^{\mathbf{MeAr}}$, $\mathbf{2}^{\mathbf{EtAr}}$, $\mathbf{2}^{\mathbf{\textit{i}PrAr}}$, and $\mathbf{2}^{\mathbf{Dip}}$.

EPR Spectra

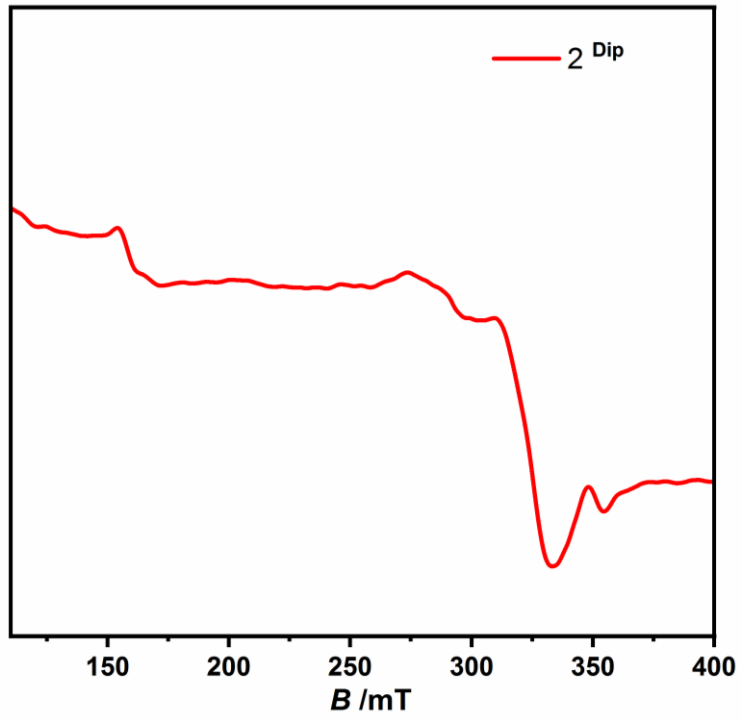

Figure S15. EPR spectrum of **2**^{Dip} measured in solid state at −175 °C.

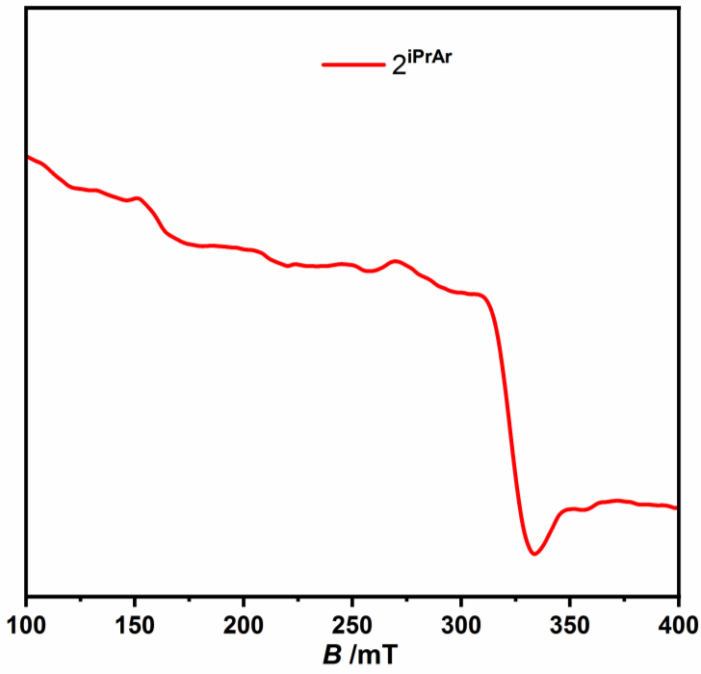

Figure S16. EPR spectrum of **2**^{iPrAr} measured in solid state at −175 °C

FT-IR Spectra

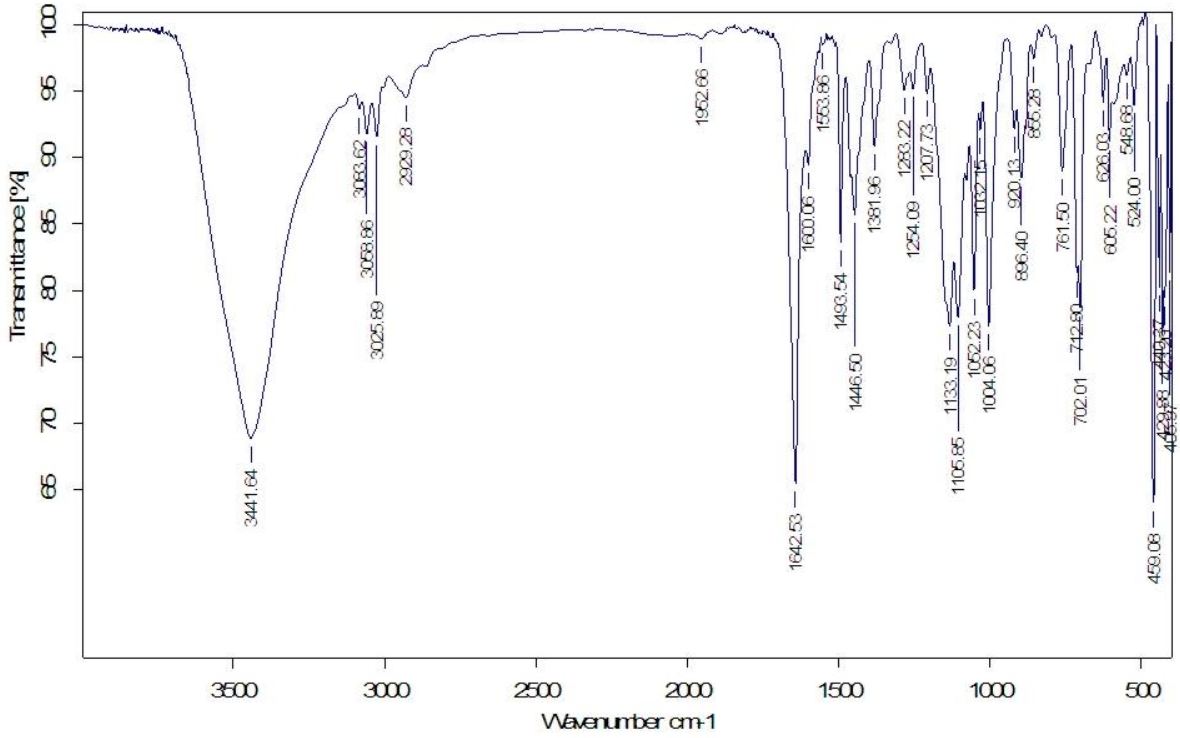

Figure S17. FT-IR of $\mathbf{2^{MeAr}}$.

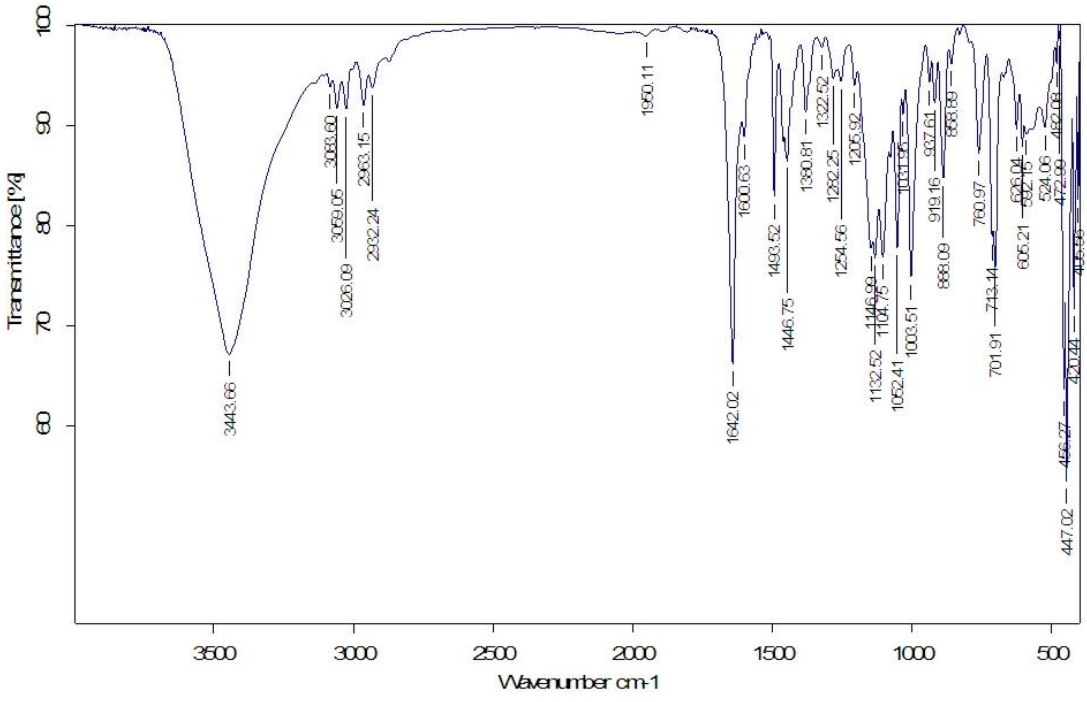

Figure S18. FT-IR of $\mathbf{2^{EtAr}}$.

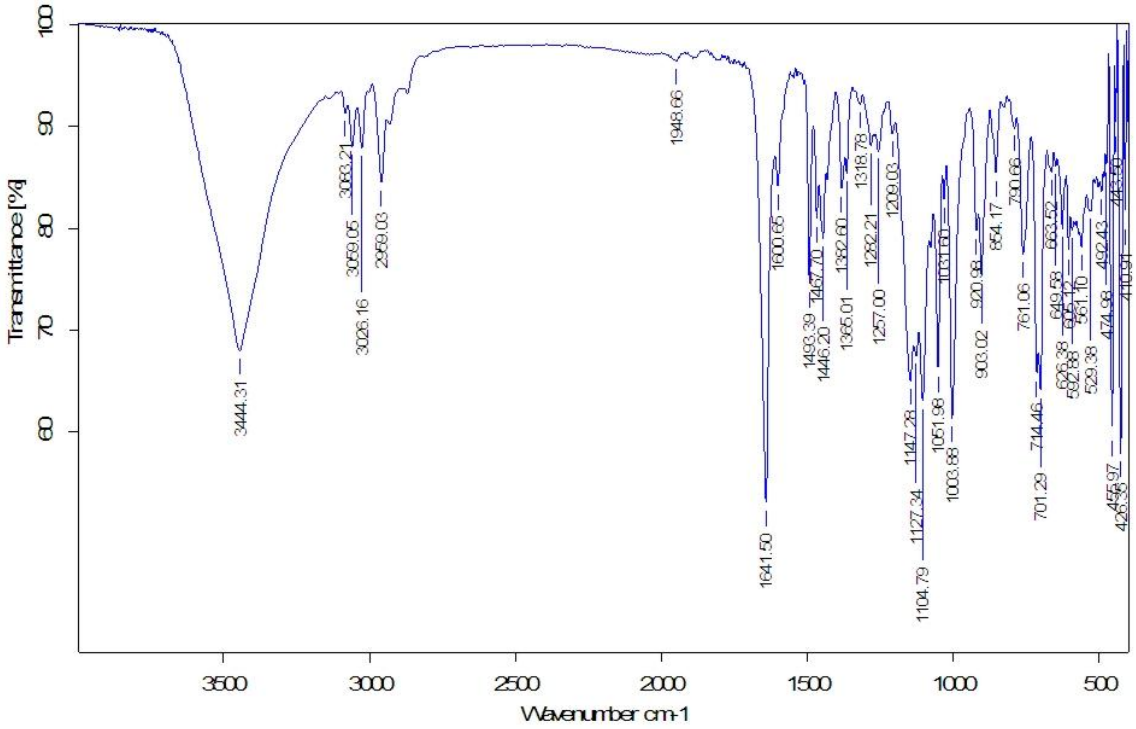

Figure S19. FT-IR of **2**^{iPrAr}.

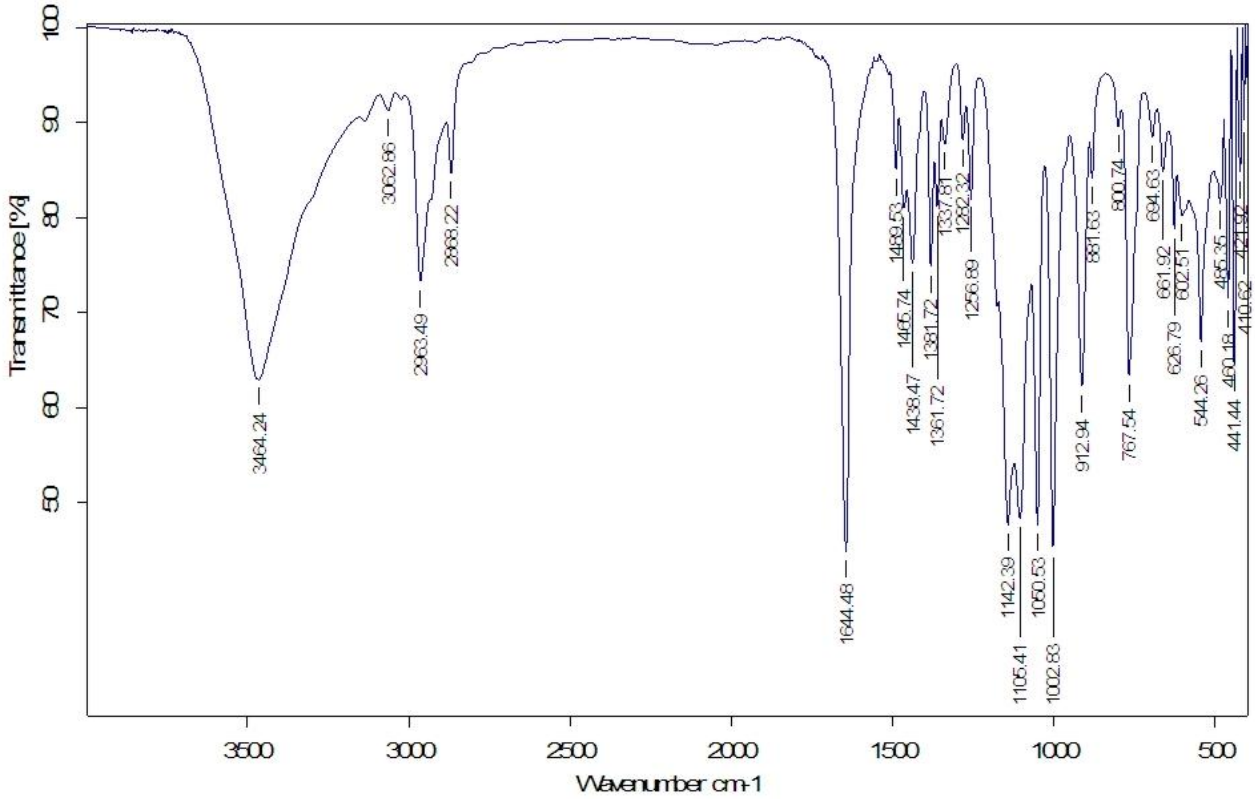

Figure S20. FT-IR of **2**^{Dip}.

CHN Data

Date of report: 5/3/2018 1:41 PM
User ID: Administrator

Run Details				Results				
Run	Run #	Weight	Created on	Carbon	Hydrogen	Nitrogen	Sulfur	Oxygen
ME CU9		1.510	5/3/2018 1:40:49 PM	56.53%	4.51%	6.69%		
IPR CU9		1.450	5/3/2018 1:35:01 PM	57.03%	4.80%	6.51%		
ET CU9		1.410	5/3/2018 1:29:06 PM	56.51%	4.68%	6.72%		
DI CU9		1.500	5/3/2018 1:23:01 PM	39.21%	4.86%	9.15%		

Figure S21. Elemental analysis results of $\mathbf{2}^{\mathbf{MeAr}}$, $\mathbf{2}^{\mathbf{EtAr}}$, $\mathbf{2}^{\mathbf{\textit{i}PrAr}}$, and $\mathbf{2}^{\mathbf{Dip}}$.

.